Vol. 140: 217–226, 1996 | MARINE ECOLOGY PROGRESS SERIES
Mar Ecol Prog Ser | Published September 12

Planar optrodes: a new tool for fine scale measurements of two-dimensional O_2 distribution in benthic communities

Ronnie Nøhr Glud[1,*], Niels Birger Ramsing[1,2], Jens Kristian Gundersen[1,2], Ingo Klimant[1]

[1]Max Planck Institute for Marine Microbiology, Microsensor Research Group, Celsiusstraße 1, D-28359 Bremen, Germany

[2]Institute of Biological Sciences, Department of Microbial Ecology, University of Aarhus, Ny Munkegade, DK-8000 Aarhus C, Denmark

ABSTRACT: A new tool ('planar optrodes') for measuring fine scale 2-dimensional O_2 distributions in benthic communities is presented and discussed. The sensor consists of an O_2-quenchable fluorophore cast onto a 25 × 55 mm, 175 µm thick transparent PVC sheet, which can be introduced into sediments and microbial mats. The O_2 sensitive fluorescence emitted by the planar optrode was measured with a high resolution CCD camera. A 3-point calibration was performed for each pixel in the acquired images to calculate the 2-dimensional oxygen distribution with high accuracy. Calibrated images covered an area of 13 × 17 mm and the set-up allowed the 2-dimensional distribution of O_2 to be resolved with a spatial resolution of 26 µm. The sensitivity of the sensor had excellent long-term stability. The planar optrode was used to record the oxygen equilibration between small gas bubbles and surrounding water with a temporal resolution of 20 s. The sensor was also used to measure the vertical and horizontal O_2 distribution in an intertidal sediment. The obtained distribution correlated well with O_2 concentration microprofiles measured with an O_2 microelectrode. The data showed pronounced differences in the O_2 penetration depths due to patchy distribution of highly labile organic carbon and showed differences in thickness of the diffusive boundary layer due to small topographic structures on the sediment surface. Potential applications of the planar optrode are presented and discussed.

KEY WORDS: O_2-microprofiles · Optrodes · Two-dimensional O_2 distribution · Sediments · Respiration

INTRODUCTION

Oxygen plays a key role in benthic microbial ecology, and flux rates of O_2 have been used to quantify primary production, total community respiration, and mineralisation rates (e.g. Smith 1978, Revsbech et al. 1981). Common techniques for such studies include O_2 exchange measurements in laboratory-incubated cores, or *in situ* measurements using benthic flux chamber landers (e.g. Hunding & Hargrave 1973, Smith et al. 1983, Glud et al. 1994b). These techniques, however, do not probe into the sediment and hence give only a limited understanding of the processes taking place at the sediment-water interface or within the sediment. The introduction of O_2 microelectrodes to microbial ecology has allowed benthic O_2 distribution to be studied with a very high temporal and spatial resolution (Revsbech et al. 1980) which has subsequently increased our understanding of O_2 dynamics in different benthic communities (e.g. Revsbech et al. 1983, Glud et al. 1992, Rasmussen & Jørgensen 1992, Canfield & Des Marais 1993, Kühl et al. 1995). By the use of microelectrodes it has also been possible to demonstrate the presence and the importance of a diffusive boundary layer (DBL), within the viscous sublayer above the sediment surface, which may impede the availability of O_2 to benthic microbial communities (Jørgensen & Revsbech 1985, Gundersen & Jørgensen 1990, Glud et al. 1994a).

Typical O_2 microelectrodes have the advantages of a small tip diameter of <10 µm, a 90% response time of <1 s, and a stirring sensitivity of <1% (Revsbech 1989).

*E-mail: ronnie@postgate.mpi-mm.uni-bremen.de

These characteristics make O_2 microelectrodes ideal for many applications in benthic microbiology. A new type of fiber optic O_2 microsensor (microoptrode), which can complement the O_2 microelectrode, has just been introduced into the field of aquatic biology (Klimant et al. 1995). The main advantages of this new sensor type compared to O_2 microelectrodes are a simpler and less time consuming construction procedure and a superior long-term stability (Klimant & Wolfbeis 1995, Klimant et al. 1995).

Both microelectrodes and microoptrodes measure the O_2 concentration at a single point, and depth profiles are obtained by a stepwise movement of the sensor up or down through the medium. Measuring several profiles in order to overcome or to describe temporal and spatial heterogeneity in benthic communities is a tedious job. Simultaneous measurement of temporal changes in O_2 concentrations at several points requires a series of sensors with associated recording devices, which is expensive and in most cases impractical. Describing 2-dimensional O_2 dynamics in heterogeneous communities, e.g. around inhabited animal burrows, in heavily bioturbated communities and in the rhizosphere using conventional microsensors, is thus a very difficult and time-consuming if not impossible task.

Here we present and demonstrate a new technique for investigating benthic O_2 concentrations and dynamics at a high spatial resolution in 2 dimensions. The technique takes advantage of an O_2-quenchable fluorophore which can be cast into thin sheets, 'planar optrodes'. These can be introduced into benthic communities to quantify the O_2 distribution next to the sheet.

MATERIALS AND METHODS

The measuring principle of the O_2 optrode is based on the ability of oxygen to act as a dynamic fluorescence quencher that decreases the fluorescence quantum yield of an immobilised fluorophore (Kautsky 1939). The fluorophore is excited by blue light with a defined short wavelength, and a red luminescent light is emitted by the fluorophore. In the presence of O_2 the intensity of the luminescent light decreases in a predictable way due to the quenching process. In contrast to O_2 microelectrodes the calibration curve for fluorescent O_2 sensors is non-linear, but can, in ideal systems, be described by the Stern-Volmer equation:

$$\frac{I_0}{I} = 1 - K_{SV} C \qquad (1)$$

where I_0 and I are the fluorescence intensities in the absence and presence of O_2 respectively, K_{SV} is the quenching constant expressing the quenching efficiency and C is the oxygen concentration (Stern & Volmer 1919).

Planar oxygen optrode. The oxygen-quenchable fluorophore ruthenium(II)-tris-4,7-diphenyl-1,10-phenathroline perchlorate was dissolved in plasticized PVC as described by Preiniger et al. (1994). This fluorophore absorbs blue light (450 nm) and emits red light with an intensity maximum at 610 nm. The mechanical stability and the back scatter intensity were enhanced by adding titanium dioxide grains (diameter approx. 1 µm) to the indicator/polymer solution (Klimant & Wolfbeis 1995). The solution was coated onto a transparent 175 µm thick polyester support foil, which was practically impermeable for O_2. The 10 µm thick sensing layer was coated by a 20 µm thick layer of black silicone to ensure optical insulation. The total thickness of the sheet was 205 µm. The fluorophore solution and the silicone coating were applied by knife-coating. During coating the support foil was kept in place by a vacuum, while spacers of 10 µm ensured the correct distance between the knife and the foil. After 4 d of silicone curing, the sheet, called here a planar optrode, was cut into 25 × 55 mm pieces ready for use.

Experimental set up. The planar optrode was glued with transparent silicone to the inside of a small frame (8 × 8 × 13 cm) constructed of transparent Plexiglas. The planar optrode was excited by light from a halogen lamp equipped with a blue glass filter (BG 12, Schott, Germany) to eliminate any red light from the excitation beam (Fig. 1). The luminescent light emitted by the planar optrode was collected by a Photometrics CCD camera (CH250L) after passing through a long-

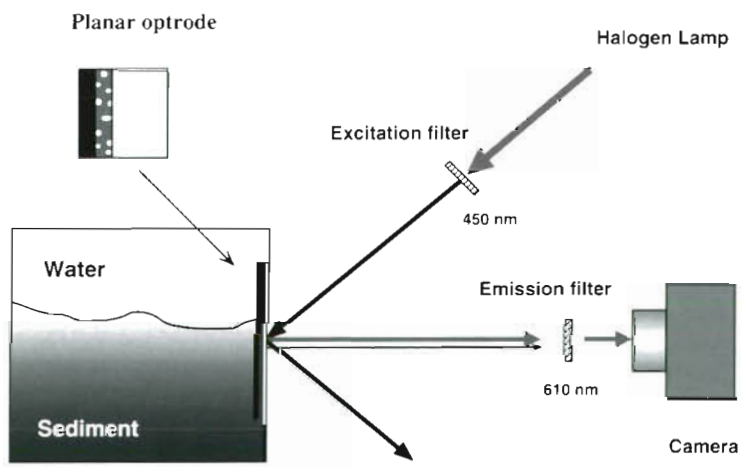

Fig. 1. Illustration of the experimental setup (not to scale). An enlargement of the 3-layered planar optrode (support foil, sensing layer, silicone layer) is shown in the upper left corner

pass glass filter (OG 570, Schott) to remove any reflected light from the excitation source. The optical insulation (the black silicone layer) ensured that no light reached the inside of the test aquarium (the frame with an applied bottom). The camera, equipped with a 60 mm Nikon macro lens and a Peltier cooled CCD chip (KAF 1400, 1317 × 1035 pixels, 6.8 × 6.8 µm), was controlled by a Macintosh Quadra computer. The images were acquired using an aperture of 5.6 f and an exposure time of 0.06 s. The digital transmission of an image from the camera to the computer took 1.7 s, which set an upper limit of the frequency with which images could be obtained. Digital pictures were acquired as 12 bit grey scale images with the program NU 200, Photometrics, and stored in 16 bit TIFF format for later analysis. All experiments were performed in a darkened room at 20°C.

The initial calibration and test of the planar optrode were performed after filling the aquarium with sea water. The O_2 concentration of the water was regulated by a 2 channel digital gas mixer (Brooks Instruments, model 5876), which flushed the aquarium with a given O_2/N_2 gas mixture through a bubbling stone. The O_2 concentration was checked by Winkler titration (Strickland & Parson 1972). After the initial calibration, an undisturbed core of sediment (30 × 30 cm) collected in a tidal area on the coast near Bremerhaven (Germany) was subcored using the small frame. This was done by slowly pressing the frame with bevelled sides into the sediment and, after recovery, sealing the bottom. The aquarium was placed in the set-up again, and water from the sampling location was added (salinity 22‰) (Fig. 1). Camera, filters, lamp and aquarium were placed in a custom-designed rack which stabilised the instrument, and ensured that all components were fixed during the experiment. Water flow above the sediment was created by directing an O_2/N_2 mixed gas stream from the gas mixer against the water surface upstream from the planar optrode. Measurements were performed 15 h after the initial setup.

A Clark-type O_2 microelectrode equipped with an internal reference and a guard cathode (Revsbech 1989) was used to continuously monitor the O_2 concentration in the water phase and to measure O_2 microprofiles. The microsensor had an outer tip diameter of 7 µm, a 90% response time of 0.5 s and a stirring sensitivity of 1%. The sensor was positioned by a micromanipulator and the sensor current was measured by a picoammeter connected to a strip chart recorder (Revsbech & Jørgensen 1986).

Image recording and analysis. The original light intensity value for each pixel in the image was quantified on a 12 bit linear grey scale from 0 to 4095. However, for further analysis and presentation, the dynamic range of intensity values used in each picture was rescaled linearly to an 8 bit grey scale (0 to 255) and the information about the individual scaling factors used for each picture was stored. For visualisation we have chosen to transform the grey scale into a linear colour scale with 256 colours in Figs. 5 & 6. In order to reduce CPU time, images were obtained with a binding factor of 2, implying that only an average value for each set of 4 neighbouring pixels was stored. This reduced the original number of pixels in the image from 1.36×10^6 to 3.40×10^5. The obtained images covered an area of 17.0 × 13.3 mm (except for those in Fig. 6). Both the horizontal and vertical spatial resolutions were consequently 26 µm. All image analyses were performed in the program NIH Image version 1.58, which is a full-featured image analysis program written by Wayne Rasband, NIH, Washington, DC, USA. The program is freely available from the anonymous FTP site *zippy.nimh.nih.gov* on the internet.

Diffusive flux calculations. The 1-dimensional diffusive O_2 uptake (J) was calculated by Fick's first law of diffusion: $J = -D_0[\partial C(z)/\partial z]$, where D_0 is the diffusion coefficient of O_2 in water, taken from Broecker & Peng (1974), and $\partial C(z)/\partial z$ is the slope of the concentration gradient (Crank 1983). No porosity correction was applied since the concentration gradient for the DBL was used.

RESULTS

The average fluorescence intensity of the planar optrode recorded as a function of O_2 saturation in the water phase is shown in Fig. 2A. The intensity declined from the initial value of 2956 ± 182 (arbitrary units on a scale from 0 to 4095) as O_2 was added to the water. At higher O_2 saturation the sensitivity of the planar optrode is reduced, which resulted in a hyperbolic decrease in intensity with increasing O_2 saturation (Fig. 2A). The standard deviation of fluorescence intensity was 5 to 8 % of the average fluorescence signal of all pixels (Fig. 2A). The relatively large variations were caused by heterogeneity in the planar optrode, mainly due to an uneven distribution of fluorophore on the polyester foil, agglutination of titanium grains, and an uneven distribution of the clear silicone used to fix the planar optrode to the aquarium wall. The heterogeneity in the fluorescent film can be recognised as a black horizontal band, black dots and fine vertical white/black lines in the images presented in Fig. 2. The calibration procedure was repeated 4 times, each time giving the same calibration curve.

The simple Stern-Volmer equation presented in the 'Materials and methods' is only strictly valid for ideal systems such as the quenching of dilute solutions of fluorophores. It has, however, been shown that a

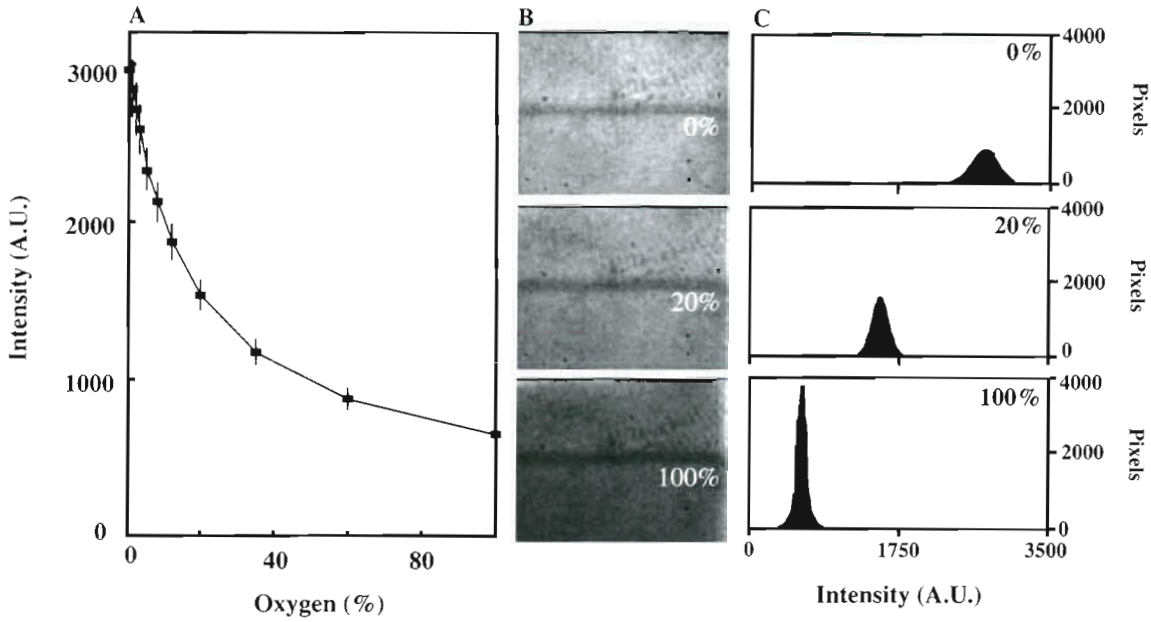

Fig. 2. (A) Average fluorescence intensity expressed on a fixed grey scale (0 to 4095 arbitrary units, A.U.) as a function of O_2 saturation in the water. The standard deviation between individual pixels is shown as error bars. (B) Three images obtained at 0, 20 and 100% O_2 saturation, and (C) the corresponding histograms of the intensity values

slightly modified Stern-Volmer equation adequately describes the response of most optrodes (Klimant et al. 1995):

$$I = I_0\left[\alpha + (1-\alpha)\left(\frac{1}{1+K_{SV}C}\right)\right] \quad (2)$$

where α is the non-quenchable fraction of the fluorescence including scattered stray light, and I_0 is the fluorescence intensity in the absence of O_2. The 2 constants α and K_{SV} are determined from 2 additional calibration points with O_2 concentrations C_1 and C_2, giving intensities I_1 and I_2, respectively, and rearranging Eq. (2) gives:

$$K_{SV} = \frac{I_0(C_2 - C_1) - (I_1C_2 - I_2C_1)}{(I_1 - I_2)C_1C_2} \quad (3)$$

$$\alpha = \frac{I(1 + K_{SV}C_1) - I_0}{I_0 K_{SV} C_1} \quad (4)$$

Using the fluorescence intensities obtained at 0, 20 and 100% O_2 saturation (Fig 2B), we measured I_0 and calculated the α and K_{SV} values for each pixel in the image of the planar optrode (Fig. 3). The average values of α and K_{SV} were 7.5 ± 1% and 53.7 ± 4.4 μM^{-1}, respectively. The observed variation in the calibration constants was mainly caused by the heterogeneity in the planar optrode. Pixels along the edge of the optrode had anomalousy high α and low K_{SV} values, which are reflected by the 2 tails in the histograms of Fig. 3. The variation between pixels was too large to allow either α, K_{SV} or I_0 to be treated as universal con-

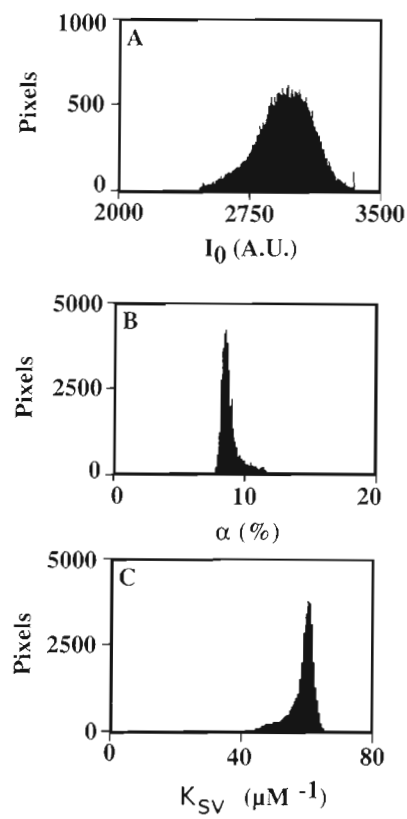

Fig. 3. Histograms of single pixel values of I_0, α and K_{SV} for the 3 calibration images presented in Fig. 2B. The values of I_0 varied from 2454 to 3366 (arbitrary units, A.U.), α varied from 2.80 to 15.07%, while the maximum and minimum values of K_{SV} were 26.07 and 68.4 μM^{-1}, respectively

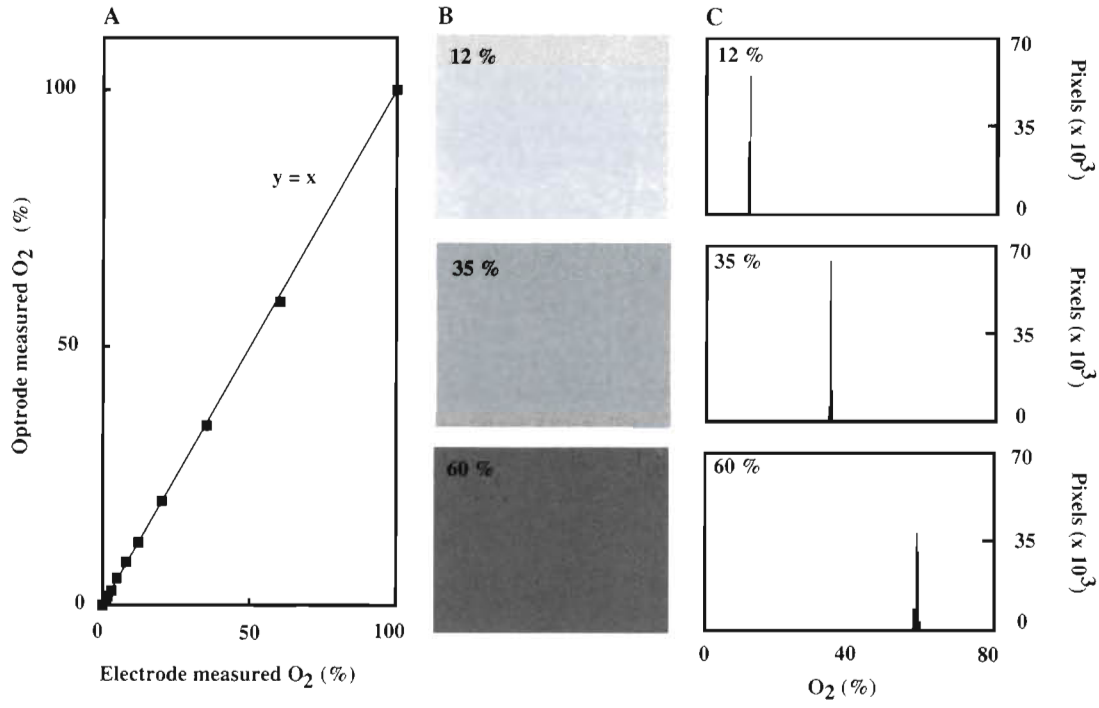

Fig. 4. (A) Average O_2 concentration measured by the planar optrode as a function of the actual O_2 concentration measured by a microelectrode. The standard deviation at each calibration point was proportional to the measured concentration (about 3% of the measured value). The error bars are consequently smaller than the symbols. The linear regression coefficient is $r^2 = 0.999$. (B) Three examples of O_2 images measured with the optrode at 12, 35 and 60% O_2 saturation, and (C) the corresponding histograms of the calibrated pixel values. The O_2 concentration is expressed on a linear grey scale from 0 to 255; each increment in intensity value corresponds to an increase in O_2 saturation of 0.48%

stants throughout the image thus necessitating an individual 3 point calibration for each pixel. Having estimated the α, K_{SV} and I_0 for each pixel, Eq. (2) was rearranged to calculate the O_2 concentration at each pixel:

$$C = \frac{I_0 - I}{K_{SV}(I - I_0\alpha)} \quad (5)$$

The average O_2 concentration of the resulting oxygen images corresponded exactly to the actual O_2 concentration in the water phase as measured by the calibrated microelectrode (Fig. 4A), and the relative variation in the intensity values between pixels in the original images was significantly reduced after calibration (Fig. 4). Three oxygen images of the planar optrode are presented in Fig. 4, together with the corresponding histograms of the pixel values; both reflect the precision of the O_2 concentration estimate.

After the calibration procedure, the O_2 concentration in the aquarium was lowered by flushing with N_2. As the O_2 concentration decreased, images were recorded every 20 s together with the read-out of the microelectrode (Fig. 5). After 270 s, the signal of the O_2 microsensor reached 0% saturation, while the planar optrode reached this value in areas without bubbles approximately 90 s later (Fig. 5A). Before flushing with N_2, bubbles had attached themselves to the surface of the optrode. The O_2 concentration also decreased inside the bubbles, but at a slower rate than in the surrounding water due to slow equilibration across the DBL surrounding the gas bubbles. The bubbles thus became visible as differently coloured areas on the images (Fig. 5). Large bubbles exhibited a slower equilibration time with the surrounding water as compared to smaller bubbles due to a higher volume/surface area ratio (Fig. 5).

Sediment was subsequently introduced into the aquarium, with a minimum of disturbance, and the overlying water was flushed with a gas mixture, leaving 12% O_2 saturation in the overlying water for 2 h to allow time for equilibration. Images were then acquired and the O_2 saturation was increased to 24%. After an additional 1.5 h another series of images was recorded. Fig. 6A shows an O_2 image taken at 12% O_2 saturation, while Fig. 6B shows an O_2 image taken at 24% O_2 saturation. An alternative way to visualise the information in the O_2 image is shown in Fig. 6C. Here pixels in the original O_2 image having the value of 0, 4, 8, 12, 16, 20 and 24% (all ±0.2%) O_2 saturation have been darkened. The resulting isopleths of O_2 concentration values appear as dark bands in Fig. 6C. The positions of the bands were traced and copied back

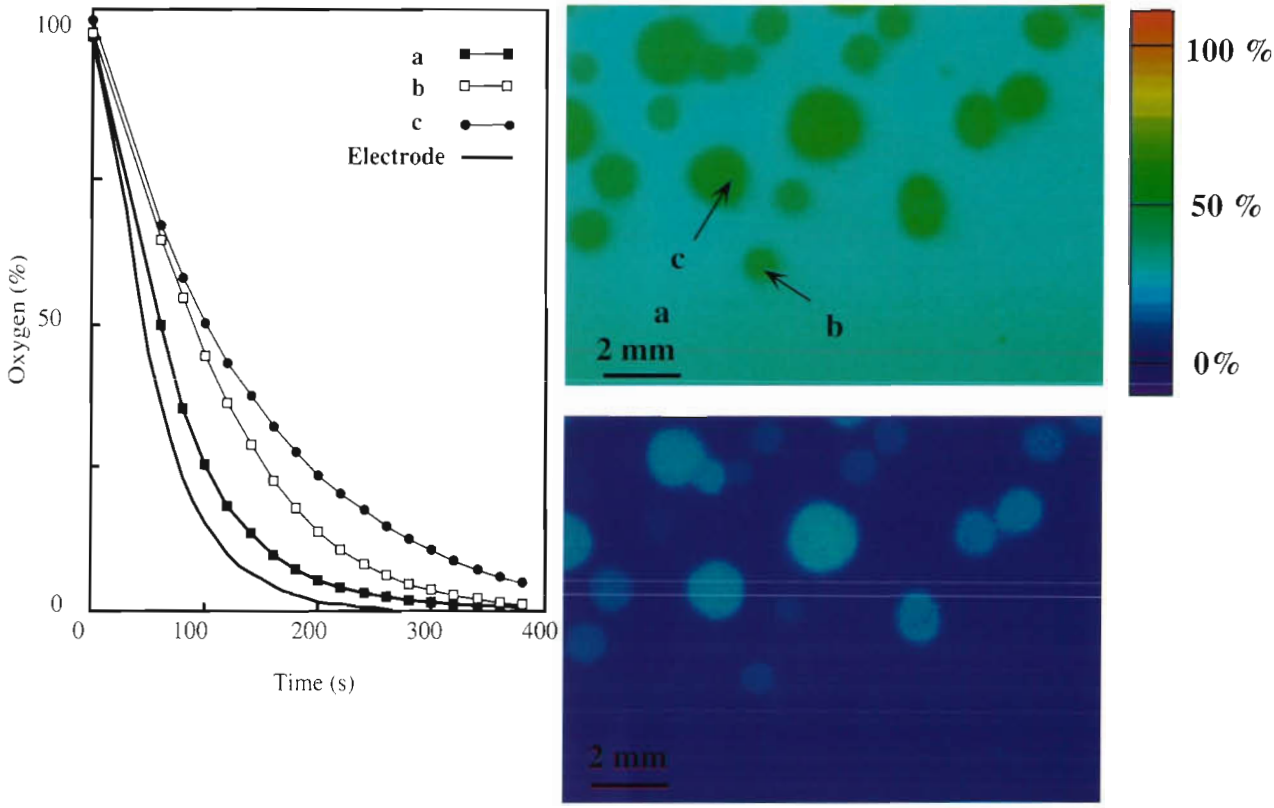

Fig. 5. (A) The O_2 concentration measured by a microelectrode (continuous line) and at 3 positions on the planar optrode (a, b and c) as a function of time after changing the flushing from O_2 to N_2. (B, C) Two oxygen images of the planar optrode obtained after 120 and 240 s, respectively. The O_2 concentration is expressed on a linear colour scale with 256 colours; scale bar is shown in the upper right corner. The gas bubbles are seen as differently coloured areas on both images

onto the original calibrated image (Fig. 6B). The same procedure was performed with the image in Fig. 6A. In order to determine the position of the sediment surface, sodium dithionite grains were deposited along the wall of the aquarium and a series of images was recorded with 3 s time intervals. The dithionite grains landed on the sediment surface and reduced any dissolved O_2 in their immediate vicinity, such that they appeared as small blue areas on the planar optrode (Fig. 6D). The sediment surface was determined by interconnecting the centres of blue areas as they first occurred in the series of pictures, and the resulting line was then copied back onto the original images (Fig. 6). Besides the image presented in Fig 6D, other images with more sodium-dithionite grains to the left and right were used for the positioning of the sediment surface.

Only to some extent did the O_2 isopleths follow the sediment topography, and consequently the O_2 penetration depth varied between 0.54 and 2.62 mm at 12% O_2 saturation, while it varied between 1.8 and 3.5 mm at 24% O_2 saturation (Fig. 6A, B). The O_2 penetration depth was smallest at the mound, which consisted of *Nereis* sp. faeces and was expected to have a relatively high O_2 consumption rate. The relative fraction of the vertical O_2 gradient present in the water phase generally increased from left to right in the image. From the oxygen images it was easy to obtain vertical O_2 microprofiles, 2 examples of which are shown in Fig. 7A and B (from positions a and b in Fig 6A). The O_2 penetration depth at these 2 positions was 1.28 and 2.59 mm and the 1-dimensional vertical diffusive O_2 uptake was 12.9 and 6.8 mmol m^{-2} d^{-1}, respectively. By increasing the O_2 saturation in the overlying water to 24%, the O_2 penetration at the same positions increased to 2.92 and 3.38 mm, while the diffusive O_2 uptake increased to 15.8 and 10.8 mmol m^{-2} d^{-1}, respectively.

By use of the microelectrode, an O_2 profile was measured at a position 2.5 mm inwards from position b on the planar optrode, at a point looking very much like the area next to the optrode. The signal was unstable in the water phase just above the sediment surface, as has been previously discussed by Jørgensen & Des Marais (1990). For that reason the electrode was positioned at each depth for 2 min and the average value of the O_2 concentration and the standard deviation at each depth were calculated as indicated by the error

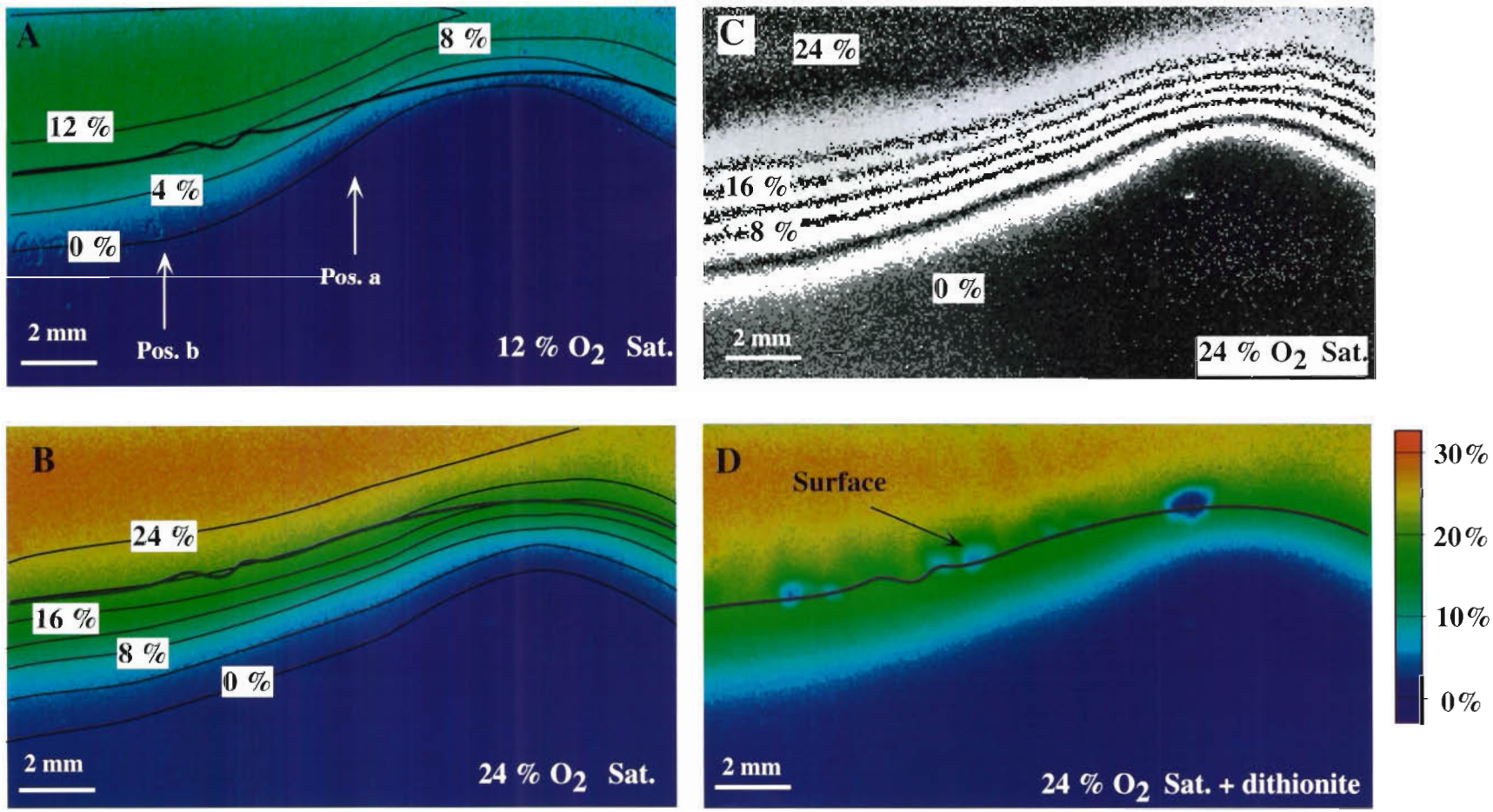

Fig. 6. Calibrated images of the O_2 distribution at the sediment-water interface with 12 % (A) and 24 % (B) O_2 saturation in the overlying water. The images represent an area of 17.0 × 10.2 mm. Sodium dithionite grains were added in order to identify the position of the sediment surface (D). For detection of the sediment surface denoted by the hatched line, several images were used along with that in D. The O_2 concentration is expressed on a linear colour scale with 256 colours and the scale bar for the images in A, B, and D is shown in the lower right corner. In (C), pixels in the original O_2 image (B) having the values 0, 4, 8, 12, 16, 20 and 24 % (all ±0.2 %) O_2 saturation have been darkened; the resulting isopleths of O_2 concentration values appear as dark bands. The isolines were copied into images A, B and C for visualisation. Flow direction was from left to right. For more details see text

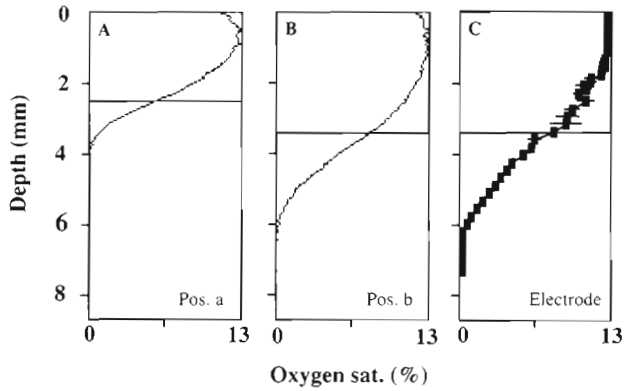

Fig. 7. (A, B) Two O_2 microprofiles obtained with the planar optrode at positions a and b in the oxygen image presented in Fig. 6A. (C) An O_2 profile measured by a microelectrode 2.5 mm inwards from the optrode surface at position a in Fig. 6A. Thick horizontal lines indicate the position of the sediment surface

bars in Fig. 7C. The instability decreased to an insignificant level below the visually determined sediment surface (Fig. 7C). The O_2 penetration depth and the diffusive O_2 uptake derived from the microelectrode profile were 2.73 mm and 6.5 mmol m^{-2} d^{-1}, respectively, with 12% O_2 saturation in the overlying water.

After the measurements the sediment was gently removed in front of the planar optrode and the optrode was recalibrated once more by flushing the water phase with N_2, atmospheric air and O_2 and acquiring images under each of these conditions. These calibration images were used to calculate the O_2 images presented in Fig. 6.

DISCUSSION

The fluorophore distribution in the planar optrode presented here was rather heterogeneous and the uneven layer of transparent silicone used to fix the optrode to the aquarium wall further increased the spatial fluctuation in the intensity values obtained at a given O_2 saturation. Another experimental difficulty was the unevenness of the light field used to excite the planar optrode, so that even small disturbances of the halogen lamp during the experiment could reduce the accuracy and reproducibility of the measurements. It was extremely important to avoid mechanical disturbances of the aquarium and the camera, and a sturdy mounting of each component in the setup relative to the others was critical. Even the slightest rotation of the camera relative to the film would result in an unacceptable displacement of the image (e.g a rotation of 0.01° means a displacement by more than 2 pixels). Despite these difficulties, we found that the applied 3-point calibration of each pixel of the images gave a reliable and constant calibration. The stability of optrodes is excellent; they maintain constant sensitivity even after extended periods of measuring (Klimant et al. 1995). The planar optrode described here showed no significant change in the calibration values after 7 h of measurements. Even after 3 mo of storage the sensitivity of the planar optrode was unchanged (data not shown).

Previous studies of the same ruthenium complex as used here showed that quenching was not affected by CO_2, H_2S, Fe^{2+}, H^+ or NaCl in ecologically relevant concentrations (Klimant & Wolfbeis 1995, Klimant et al. 1995). However, both the unquenched fluorescent intensity (I_0) and the quenching coefficient (K_{SV}) are temperature dependent. Microoptrodes, based on the ruthenium complex dissolved in plasticized PVC, exhibited a decrease in fluorescence intensity (I_0) of approximately 0.5% and an increase in K_{SV} of around 1% per °C temperature increase. Changes in temperature therefore have to be taken into account when images are calibrated. Optrodes do not, as electrodes, consume O_2 and the signal is therefore not sensitive to stirring (Revsbech 1989).

In water-saturated air, the response time of the planar optrode was less than a second (data not shown). The apparent response time of the planar optrode as measured by the experiment presented in Fig. 5 was, however, approximately 90 s. This difference is presumably caused by the presence of a DBL in front of the submerged planar optrode as compared to the planar optrode in air. As for any other submerged surface, the DBL will cover the planar optrode and any adhesive bubbles like a carpet (Gundersen & Jørgensen 1990, Jørgensen & Des Marais 1990). Consequently, as the O_2 concentration in the turbulent water phase changes, it takes time before a new steady-state O_2 profile throughout the DBL, the 20 µm thick silicone layer and the 10 µm thick sensing layer has been re-established. The response time of a planar optrode is therefore highly dependent upon the thickness of the DBL and thus upon the flow velocity of the free-flowing water in front of the planar optrode. Single pixels situated between bubbles, where the DBL was expected to be thicker, did indeed also show a slower response than the pixels situated at position a in Fig. 5 (data not shown). The time for changing the gas mixing from O_2 to N_2 was not defined better than 5 s and the mixing of the water phase by the flushing may not have been ideal. This could have slightly affected the data presented in Fig. 5.

The response time of a planar optrode in sediment is, however, the same as in water-saturated air (i.e. <1 s) since any change in O_2 concentration in front of the optrode only has to equilibrate through the silicone

layer. This was partly verified since deposition of dithionite crystals on the sediment surface directly in front of the planar optrode resulted in complete O_2 depletion around the crystals in <3 s (data not shown). The apparent response time for processes occurring right next to the optrode surface must thus be less than 3 s.

The possibility that smearing occurred during sediment coring could not be excluded; however, we did not observe any smearing along the transparent parts of the aquarium. Further, the similarities between the profile obtained by the microelectrode and the planar optrode suggest that smearing was a minor problem.

The O_2 data at the sediment water interface (Figs. 6 & 7) were obtained with the planar optrode fixed on a wall of the aquarium, resulting in very complex hydrodynamic conditions at the sediment-water-wall interface. Care must therefore be taken when interpreting the data within the DBL and in the very upper part of the sediment. It was, however, clear that the relative fraction of the O_2 gradient present in the water phase was larger downstream than upstream from the mound (especially noticeable in Fig. 6B), indicating, as expected, the presence of a thicker DBL on the lee side of the mound (Gundersen & Jørgensen 1990). The concentration gradient of the vertical O_2 optrode profiles also exhibited a break at the sediment interface due to changed diffusive conditions going from the water phase into the sediment (Glud et al. 1995). The diffusive O_2 uptake and the O_2 penetration depth determined from the images at positions a and b (Fig. 6A) were in the expected range for an organically rich coastal sediment (Rasmussen & Jørgensen 1992). Increasing O_2 concentrations and the presence of easily degradable organic carbon (*Nereis* faeces) also increased the diffusive O_2 uptake and increased/decreased the O_2 penetration depth as expected.

The instability of the O_2 signal in the DBL as measured by the microelectrode was probably caused by eddies intruding into the unstable DBL from the overlying turbulent water phase (Gundersen & Jørgensen 1990). The vertical profiles obtained by the planar optrode were smoother and the signal was more stable in the DBL due to the slower response time in the water phase. The optrode profile and the microelectrode profile measured close to position b were very similar, except for the stability in the DBL, validating the data obtained by the planar optrode.

The planar optrodes have especially good prospects for studies in systems where the hydrodynamic conditions at the sediment-water interface are of minor importance but where the spatial and temporal variation in O_2 concentration is high. Examples of such systems could be: rhizospheres, permeable sediments with advective porewater transport, heavily bioturbated sediments and ventilated worm burrows where traditional microsensors only give very limited information about the 2-dimensional O_2 dynamics. Another option would be to let biofilms develop directly on planar optrodes so that the dynamics of anoxic microniches at the base of a biofilm (De Beer et al. 1994) could be studied as a function of different parameters. Potentially the combination of planar optrodes and the light-dark shift technique (Revsbech et al. 1981, Glud et al. 1992) would allow photosynthesis and photosynthesis-coupled respiration to be quantified in 2 dimensions in microbial mats and light-induced migration of activity zones could be followed.

Planar optrodes have for some years been applied within the fields of medicine and physiology (Leiner 1991, Lübbers et al. 1995). However, the study presented here is the first attempt to use the O_2 sensitive layer for O_2 imaging, and the data demonstrate that planar optrodes are powerful tools for describing and quantifying 2-dimensional O_2 distribution in benthic microbial systems.

Acknowledgements. We thank Garby Eickert for construction and test of the microelectrode and Axel Krack for skilful assistance. We also hank Wayne Rasband for writing and continuously updating his excellent public domain image analysis program, NIH Image. Bo Barker Jørgensen and Michael Kühl are thanked for valuable criticism of the manuscript. This work was supported by the Max Planck Gesellschaft, through the Biotechnology Programme (Biotek 2) by the Danish Research Councils, and by the European Union (project: MICROMARE; Contract MASCT 950029).

LITERATURE CITED

Broecker WS, Peng TH (1974) Gas exchange rates between air and sea. Tellus 26:21–35

Canfield DE, Des Marais DJ (1993) Biogeochemical cycles of carbon, sulphur and free oxygen in a microbial mat. Geochim Cosmochim Acta 57:3971–3984

Crank J (1983) The mathematics of diffusion. Clarendon, Oxford

De Beer D, Stoodley P, Roe F, Lewandowski Z (1994) Effects of biofilm structures on oxygen distribution and mass transport. Biotech Bioeng 43:1131–1138

Glud RN, Gundersen JK, Jørgensen BB, Revsbech NP (1994a) Effects on the benthic diffusive boundary layer imposed by microelectrodes. Limnol Oceanogr 39:462–467

Glud RN, Gundersen JK, Jørgensen BB, Revsbech NP, Schulz HD (1994b) Diffusive and total oxygen uptake of deep-sea sediments in the eastern South Atlantic Ocean: *in situ* and laboratory measurements. Deep Sea Res 41:1767–1788

Glud RN, Jensen K, Revsbech NP (1995) Diffusivity in surficial sediments and benthic mats determined by use of a combined N_2O-O_2 microsensor. Geochim Cosmochim Acta 59:231–237

Glud RN, Ramsing NB, Revsbech NP (1992) Photosynthesis and photosynthesis coupled respiration in natural biofilms quantified with oxygen microsensors. J Phycol 28:51–60

Gundersen JK, Jørgensen BB (1990) Microstructure of diffusive boundary layers and the oxygen uptake of the sea floor. Nature 345:604–607

Hunding C, Hargrave BT (1973) A comparison of benthic microalgal production measured by C^{14} and oxygen methods. J Fish Res Bd Can 30:309-312

Jørgensen BB, Des Marais D (1990) The diffusive boundary layer of sediments: oxygen microgradients over a microbial mat. Limnol Oceanogr 35:1353-1355

Jørgensen BB, Revsbech NP (1985) Diffusive boundary layers and the oxygen uptake of sediments and detritus. Limnol Oceanogr 30:111-122

Kautsky H (1939) Quenching of luminescence by oxygen. Trans Faraday Soc 35:216-219

Klimant I, Meyer V, Kühl M (1995) Fiber-optic oxygen microsensors, a new tool in aquatic biology. Limnol Oceanogr 40:1159-1165

Klimant I, Wolbeis OS (1995) Oxygen sensitive luminescent materials based on silicone-soluble ruthenium diimine complexes. Analyt Chem 34:3160-3166

Kühl M, Cohen O, Dalsgaard T, Jørgensen BB, Revshbech NP (1995) Microenvironment and photosynthesis of zooxanthellae in scleractinian corals studied with microsensors for O_2, pH and light. Mar Ecol Prog Ser 117:159-172

Leiner MJP (1991) Luminescence chemical sensors for biomedical applications: scope and limitations. Analyt Chim Acta 225:209-222

Lübbers DW, Köster T, Holst GA (1995) Advances in fluorescence sensing technology II. SPIE 2388:507-518

Preiniger C, Klimant I, Wolfbeis OS (1994) An optical fiber sensor for biological oxygen demand. Analyt Chem 66: 1841-1846

Rasmussen H, Jørgensen BB (1992) Microelectrode studies of seasonal oxygen uptake in a coastal sediment: role of molecular diffusion. Mar Ecol Prog Ser 81:289-303

Revsbech NP (1989) An oxygen microelectrode with a guard cathode. Limnol Oceanogr 34:474-478

Revsbech NP, Jørgensen BB (1986) Microelectrodes: their use in microbial ecology. Adv Microb Ecol 9:293-352

Revsbech NP, Jørgensen BB, Blackburn TH, Cohen Y (1983) Microelectrode studies of photosynthesis and O_2, H_2S and pH profiles of a microbial mat. Limnol Oceanogr 28: 1062-1074

Revsbech NP, Jørgensen BB, Brix O (1981) Primary production of microalgae in sediments measured by oxygen microprofile, $H^{14}CO_3^-$ fixation and oxygen exchange methods. Limnol Oceanogr 26:717-730

Revsbech NP, Sørensen J, Blackburn TH, Lomholt JP (1980) Distribution of oxygen in marine sediments measured with microelectrodes. Limnol Oceanogr 25:403-411

Smith KL Jr (1978) Benthic community respiration in the NW Atlantic Ocean: *in situ* measurements from 40 to 5200 m. Mar Biol 47:337-347

Smith KL Jr, Laver MB, Brown NO (1983) Sediment community oxygen consumption and nutrient exchange in the central and eastern North Pacific. Limnol Oceanogr 28: 882-898

Stern O, Volmer M (1919) Über die Abklingzeit der Fluoreszenz. Phys Z 20:183-188

Strickland JD, Parsons TR (1972) A practical handbook of seawater analysis, 2nd edn. Bull Fish Res Bd Can 167

This article was submitted to the editor

Manuscript first received: February 27, 1996
Revised version accepted: May 24, 1996